# Pseudogap opening in single-crystal $YMn_4Al_8$ investigated through $^{55}$Mn and $^{27}$Al NMR measurements

Kihyeok Kang,[1] Moohee Lee,[1,*] N. H. Sung,[2] and B. K. Cho[2]
[1]*Department of Physics, Konkuk University, Seoul 05029, Republic of Korea*
[2]*School of Materials Science and Engineering, Gwangju Institute of Science and Technology, Gwangju 61005, Republic of Korea*

(Received 25 December 2017; revised manuscript received 14 November 2018; published 10 December 2018)

$^{55}$Mn and $^{27}$Al NMR measurements are performed on a single crystal of $YMn_4Al_8$, which is known as one of the rare examples of pseudogap opening in transition intermetallic compounds, to investigate the formation of this pseudogap. The NMR spectrum, Knight shift, linewidth, and spin-lattice relaxation rate $1/T_1$ are measured as functions of the temperature down to 4 K for the $c$ axis, which is parallel and perpendicular to a magnetic field of 8 T. The temperature dependencies of the Knight shifts and $1/(T_1T)$ for both NMRs as well as the magnetic susceptibility show significant decrease as the temperature decreases below room temperature, indicating the opening of a pseudogap down to ~100 K, where these data become nearly constant, confirming that the formation of the spin pseudogap is incomplete and a finite density of states remains below. By analyzing $^{55}K(T)$ and $^{27}K(T)$ thoroughly, we decompose the orbital and spin shifts for both Mn and Al sites, from which the anisotropies of the Korringa ratios are extracted. The Korringa ratios at the Mn sites are temperature dependent and highly anisotropic above 100 K, and then decrease approaching unity and become isotropic and constant below 100 K. From the temperature dependencies of $1/(T_1T)$ for both NMRs, the pseudogap temperature, $T^*$ is found to be approximately 270 K. From the anisotropy of $^{55}1/(T_1T)$ during the opening of the pseudogap, we observed that the antiferromagnetic spin fluctuation is anisotropic and stronger by up to ~4.2 times in the basal plane perpendicular to the quasi-one-dimensional (1D) manganese chain. This significant anisotropy must originate from the 1D nature of the Mn magnetic interaction.

DOI: 10.1103/PhysRevB.98.224412

## I. INTRODUCTION

The duality of the itinerant and localized characters of $d$- and $f$-electron systems often enhances orbital hybridization with conduction electrons, leading to a strong electron correlation and consequently a variety of fascinating novel phenomena such as mixed valence compounds, heavy fermion systems, unconventional superconductors, non-Fermi-liquid behavior, and spin- and charge-gap formation. Although the study of gap opening is important to reveal the underlying mechanism of this strong correlation, the observation of gap opening in real systems has rarely been reported, especially in transition-metal compounds. One such candidate system was recently reported to be the tetragonal intermetallic compound $YMn_4Al_8$ [1]. This material is known as a unique correlated electron system exhibiting unusual magnetic properties associated with the narrow spin excitation gap.

Tetragonal $RMn_4Al_8$ (where $R$ = La, Y, or Lu) compounds have the $ThMn_{12}$-type structure shown in Fig. 1 and are known as 3$d$ transition metals with strong electron correlations. $YMn_4Al_8$ is an itinerant electron magnet with a large electronic specific-heat coefficient of 83 mJ/(K$^2$ mol), and no magnetic ordering has been reported down to $T$ = 1.5 K, which is indicative of the persistence of a strong electron correlation [2]. Recent research on $YMn_4Al_8$ has drawn significant attention because of its pseudogap behavior [1,3]. Together with iron monosilicide [4] (FeSi), this system may be another candidate for a 3$d$ transition-metal compound with a correlation gap. However, $LaMn_4Al_8$ is known to be a strongly correlated electron paramagnet. As the Mn-Mn interatomic distance becomes larger, the paramagnetic properties are enhanced, and magnetic ordering below 4.5 K has been reported by muon spin rotation measurements [5].

The crystal structure of $YMn_4Al_8$ in Fig. 1 suggests a magnetic interaction of a quasi-one-dimensional (1D) nature, in which Mn atoms at the 8$f$ site form linear chains along the $c$ axis with an intrachain distance of 2.55 Å and an interchain distance of 4.43 Å [6–8]. The short distance between the nearest-neighbor Mn atoms is understood to be important for the stability of the Mn moment in Mn intermetallic compounds [9]. Figure 2 shows that the Mn(8$f$) sites have monoclinic 2/$m$ symmetry, whereas two Al sites 8$i$ and 8$j$ have orthorhombic $m2m$ symmetry.

After the low-temperature Curie tail is subtracted, the susceptibility of $YMn_4Al_8$ gradually decreases below 500 K, where it exhibits a broad maximum [10,11]. This behavior is suggested by the presence of two square bands separated by a spin pseudogap [1,3]. Unlike the magnetization, the resistivity $\rho(T)$ shows significant anisotropy [3] and its crossover occurs at $T$ = 43 K.

Although $YMn_4Al_8$ is a fascinating system and numerous papers have reported on it, many issues still need to be investigated. First, the origin of gap formation is still controversial in temperature-induced local moment scenarios, the Kondo

*Corresponding author: mhlee@konkuk.ac.kr

 

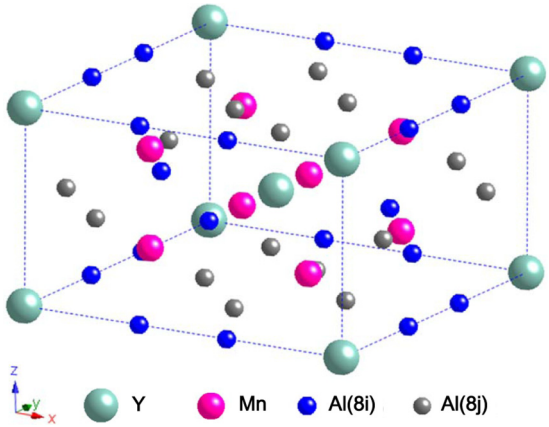


FIG. 1. Crystal structure of $YMn_4Al_8$.

insulator model, and semiconductor-metal transition. Second, the role of the 1D nature of the magnetic interaction in the gap opening is not known yet. Even the types of magnetic interactions between Mn $3d$ moments are not clearly understood. Third, from a materials point of view, it has not been confirmed whether the finite intragap density of states (DOS) is intrinsic in origin.

NMR measurements can be used to sensitively probe local electronic and magnetic structures using nuclear spins. In particular, if a spin excitation gap develops, the local field at the probed nuclear site will be significantly influenced, resulting in large changes in the NMR data such as the spectrum, shift, linewidth, and relaxation rate. Although NMR techniques have been applied to study pseudogap opening [1], previous measurements have been performed on a polycrystalline specimen, which restricts precise measurements of site-sensitive data as well as the anisotropy of local electronic and magnetic structures. Furthermore, it is important to note that only the structurally ordered $RMn_4Al_8$ shows metallic conductivity and the opening of a pseudogap is often affected by disorder and off-stoichiometry [1,12]. In addition, the Curie upturn (tail) and residual DOS after incomplete gap opening are sensitive to the concentration of paramagnetic impurities [1,3]. In short, a high-quality sample is essential for the study of this puzzling phenomenon in strongly correlated systems. Therefore, we have adopted a single-crystal $YMn_4Al_8$ sample and carried out $^{55}$Mn and $^{27}$Al NMR measurements.

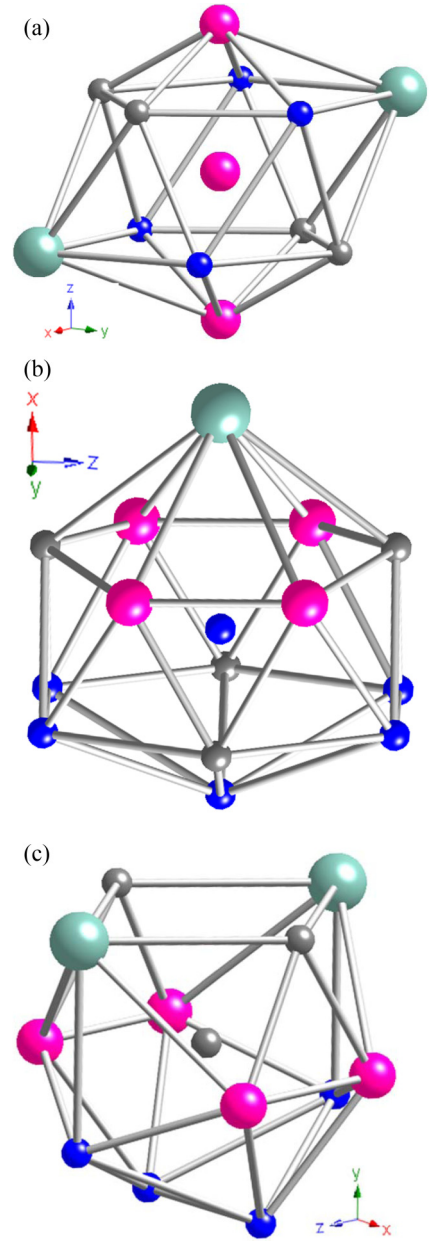


FIG. 2. (a) Local symmetry at the Mn($8f$) site. (b) Local symmetry at the Al($8i$) site. (c) Local symmetry at the Al($8j$) site.

## II. EXPERIMENTS

A single crystal of $YMn_4Al_8$ was prepared by the solution growth of a Mn–Al-rich liquid alloy [13]. The sample was identified with the space group $I4/mmm$ and had lattice parameters of $a = 8.86$ Å and $c = 5.12$ Å. The dimensions of the crystal were approximately $2 \times 4 \times 7\,\text{mm}^3$ with the largest dimension along the $c$ axis. The magnetic susceptibility was measured using a superconducting quantum interference device magnetometer at $H = 1$ kOe. Pulsed NMR measurements were carried out using a laboratory-built pulsed NMR spectrometer. The $^{55}$Mn and $^{27}$Al NMR spectra, shift, linewidth, and $1/T_1$ were measured in the range of 4–320 K at $H_0 = 8.0$ T. The nuclear spins were $I = 5/2$ for both $^{55}$Mn and $^{27}$Al. The gyromagnetic ratios were $^{55}\gamma = 10.50097$ and $^{27}\gamma = 11.09405$ MHz/T. NMR measurements were performed with the magnetic field parallel and perpendicular to the $c$ axis. The $c$ axis of $YMn_4Al_8$ was identified through x-ray-diffraction measurements. Broad spectra were obtained by scanning the spectrometer frequency with a point-by-point method at a fixed magnetic field. $1/T_1$ was measured using the saturation recovery [14] and the comb pulse [14], comb $-t - \pi/2 - \tau_0 - \pi/2 -$ echo, with varying delay times $t$ and a fixed $\tau_0$. Because the $YMn_4Al_8$ single crystal exhibited metallic conductivity, exceptional care was taken to avoid the skin-depth and eddy-current heating problems from the rf pulses.

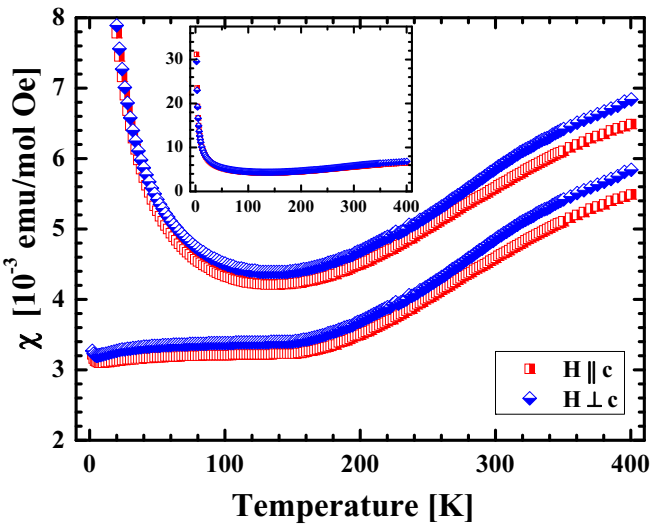


FIG. 3. Temperature-dependent magnetization divided by applied magnetic field $M(T)/H$ at $H = 1$ kOe before (upper set) and after (lower set) the subtraction of Curie term below 150 K. The upper set was shifted up intentionally by $1 \times 10^{-3}$ emu/mol Oe for clarity. Inset: All data before the subtraction in the extended range.

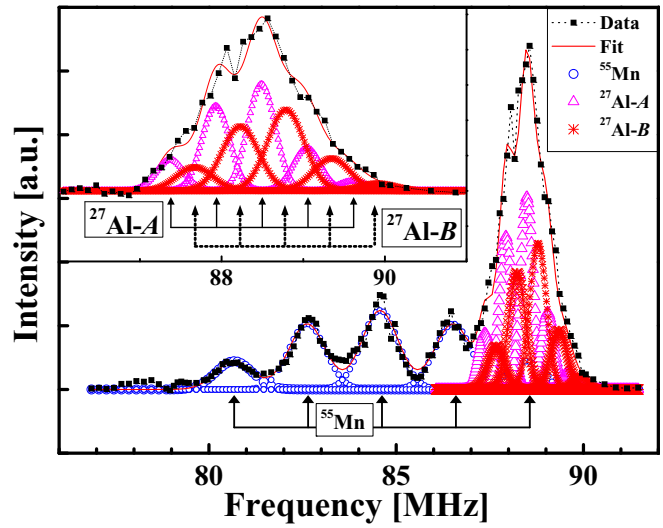


FIG. 4. $^{55}$Mn and $^{27}$Al NMR spectra for $YMn_4Al_8$ at 4.0 K with a magnetic field of 8.0 T perpendicular to the $c$ axis. The fit line is a simulated spectrum for the first-order quadrupolar splitting of two $I = 5/2$ nuclei. Three sets of five peaks are shown as guides.

## III. RESULTS AND DISCUSSION

### A. NMR spectra and linewidths

Figure 3 shows the temperature-dependent magnetization $M(T)/H$ with magnetic field applied parallel and perpendicular to the $c$ axis for a single crystal of $YMn_4Al_8$ over a temperature range of 2–400 K. The error is smaller than the size of the symbols. The $M(T)/H$ data were corrected by the subtraction of a Curie-type signal below 150 K. The Curie term can be ascribed to an extrinsic paramagnetic impurity, which was identified by the isothermal magnetization at $T = 2$ K for magnetic field up to 7 T, as described previously [3]. The anisotropy below 400 K is less than 7%, which is not significant. The data for a magnetic field parallel to the $c$ axis are consistent with the previous result [3] within the experimental error.

Figure 4 shows the $^{55}$Mn and $^{27}$Al NMR spectra at 4.0 K and 8.0 T when the $c$ axis was perpendicular to the magnetic field. The $^{55}$Mn NMR spectrum for a single crystal of a Mn-containing compound typically displays five peaks, one central and four satellites, because the six equally spaced nuclear Zeeman levels ($m = \pm 1/2$, $\pm 3/2$, and $\pm 5/2$) for the $^{55}$Mn nuclear spin of $I = 5/2$ are shifted by a first-order quadrupolar interaction [15,16]. The central peak belongs to the $+1/2 \leftrightarrow -1/2$ transition ($m = 1/2$), while the four satellite peaks arise from the $m \leftrightarrow m - 1$ transition with $m = +5/2$, $+3/2$, $-1/2$, and $-3/2$. One satellite of the $^{55}$Mn NMR spectrum overlaps with the entire $^{27}$Al NMR spectrum on the high-frequency side. The four quadrupolar satellites are symmetrically spaced at frequencies above and below the central peak with an intensity ratio of 5:8:9:8:5. The frequencies of the five peaks vary depending on the angle $\theta$ between the magnetic field and the principal axis of the electric-field gradient (EFG) tensor, i.e., the second derivatives of the potential, at the resonant nuclear position. The exact angular dependence is complicated. However, for the case where the EFG tensor has an asymmetry factor close to zero, namely, $\eta \approx 0$, the angular dependencies of the five peaks $\nu_m$ are given as $\nu_m(\theta) - \nu_n = \nu_Q\,(m - 1/2)(3\cos^2\theta - 1)/2$, where $\nu_n$ is the resonant frequency of the central peak and $\nu_Q$ is the nuclear quadrupole frequency.

From Fig. 4, the five broad peaks of $^{55}$Mn are identified and decomposed with a separation of approximately 2 MHz, which is roughly $^{55}\nu_Q/2$, as discussed later. Because the nuclear spin of $^{27}$Al is the same as that of $^{55}$Mn, $I = 5/2$, we also expect five peaks for the $^{27}$Al NMR spectrum. However, the $^{27}$Al NMR spectrum in Fig. 4 shows a single broad peak because $^{27}\nu_Q$ and the quadrupolar splitting are small, approximately 0.5 MHz, compared with the linewidth for $^{27}$Al. Furthermore, it turns out that the $^{27}$Al NMR spectrum is more complex because of the two inequivalent sites of $^{27}$Al, namely, the Al($8i$) and Al($8j$) sites. Indeed, the broad peak of $^{27}$Al at 4 K can be decomposed into two sets of five narrow peaks, as shown in the inset of Fig. 4. This decomposition is confirmed at much higher temperatures, 295 K in Fig. 5 and 320 K in Fig. 6, at which the linewidth decreases significantly.

Figure 5 shows the $^{55}$Mn and $^{27}$Al NMR spectra at 295 K and the magnetic field of 8 T perpendicular to the $c$ axis. As the temperature increases, the NMR spectra exhibit remarkable decreases in both the linewidth and intensity compared with the 4-K spectra. Even though many peaks overlap in the $^{27}$Al spectrum, which includes two Al sites and $^{55}$Mn broad satellite peaks from quadrupolar broadening, all of the peaks in the $^{27}$Al spectrum can be identified, unlike in the very broad spectra at 4 K. It is reasonable to expect a clear separation of peaks in the $^{27}$Al NMR spectrum with increasing temperature.

Therefore, we performed measurements at 320 K, as shown in Fig. 6. At elevated temperatures, the averaging of the NMR signals (typically over several tens of thousands of measurements) is required to obtain good-quality NMR data for a single crystal of $YMn_4Al_8$. In contrast with the NMR

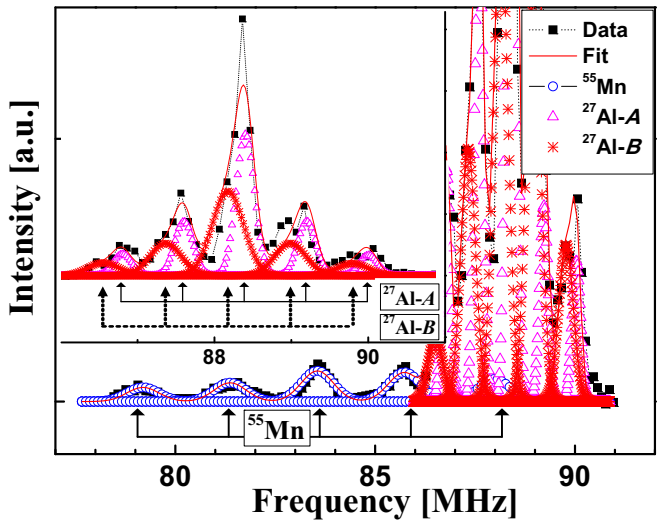


FIG. 5. $^{55}$Mn and $^{27}$Al NMR spectra for $YMn_4Al_8$ at 295 K with a magnetic field of 8.0 T perpendicular to the $c$ axis. The fit line is a simulated spectrum for the first-order quadrupolar splitting of two $I = 5/2$ nuclei. Three sets of five peaks are shown as guides.

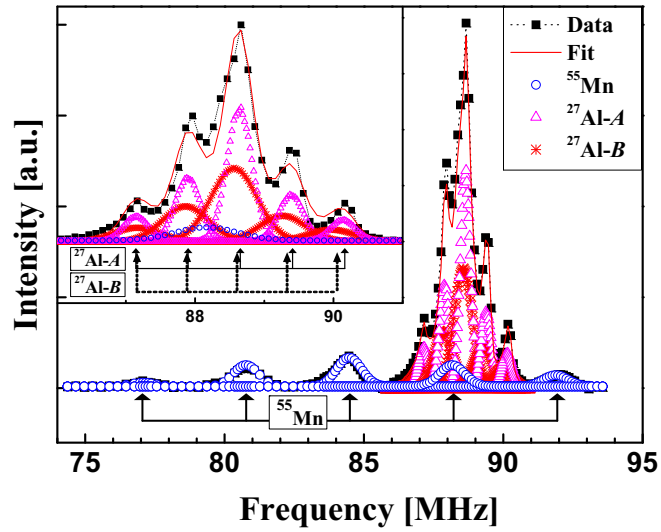


FIG. 7. $^{55}$Mn and $^{27}$Al NMR spectra of $YMn_4Al_8$ at 4.0 K with a magnetic field of 8.0 T parallel to the $c$ axis. The fit line is a simulated spectrum for the first-order quadrupolar splitting of two $I = 5/2$ nuclei. Three sets of five peaks are shown as guides.

spectra at 4 K, the spectra at 320 K clearly show the broad (Al$-A$) and still *broader*(Al$-B$)peaks. The two Al sites must have arisen from the slightly different crystallographic environments in the crystal, as shown in Figs. 2(b) and 2(c). In the case of the Al($8i$) site, each Al has four Mn atoms at 2.741 Å, whereas each of the Al($8j$) sites is located closer to four Mn atoms that are 2.569 Å away [7,8]. The Al($8i$) site is positioned 0.974 Å *above* the center, whereas the Al($8j$) site is located *almost at* the center of four Mn $3d$ moments (off by 0.11 Å). Because a local moment greatly influences the NMR linewidth via the local field inhomogeneity and the relaxation rates via the spin fluctuations (SFs), the large linewidth of the Al-$A$ and Al-$B$ peaks and the broad Mn peaks confirm

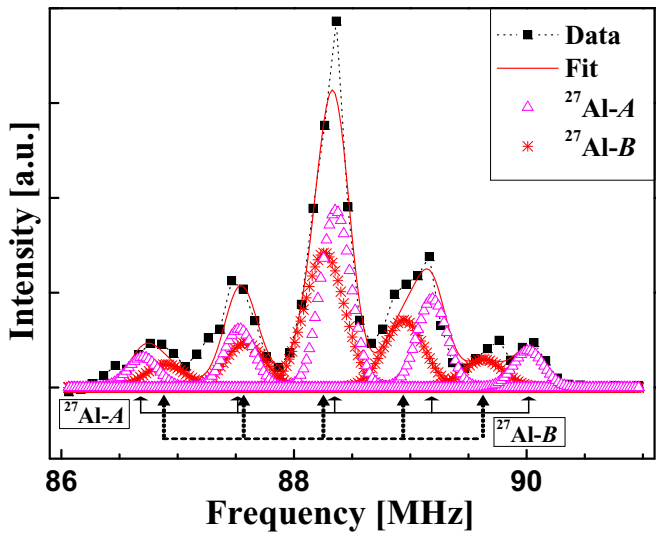


FIG. 6. $^{27}$Al NMR spectra for $YMn_4Al_8$ at 320 K with a magnetic field of 8.0 T perpendicular to the $c$ axis. The fit line is a simulated spectrum for the first-order quadrupolar splitting of the $I = 5/2$ nucleus. Two sets of five peaks are shown as guides.

that the inhomogeneous broadening of both Al-$A$ and Al-$B$ peaks originates from the Mn $3d$ local moment. Therefore, the *larger* linewidth (together with the *higher* relaxation rate explained later) of the Al-$B$ peak suggests that Al-$B$ belongs to the Al($8j$) site whereas the Al-$A$ is associated with the Al($8i$) site.

Figure 7 shows the $^{55}$Mn and $^{27}$Al NMR spectra at 4 K with a magnetic field of 8 T parallel to the $c$ axis. Notably, in contrast with the magnetic field in the perpendicular direction, the $^{27}$Al peaks in this case are separated at 4 K. The separation between the center and satellite peaks for the $^{55}$Mn NMR spectrum is nearly doubled in comparison with that for the perpendicular direction. However, the variation between the separations in the $^{27}$Al NMR spectra for the parallel and perpendicular directions is not clear. This means that the principal axis of the EFG tensor [15,16] for the $^{55}$Mn nucleus is rotated by 90°, but that for $^{27}$Al is not rotated. Thus, the principal axes of the EFG tensor for $^{55}$Mn and $^{27}$Al must be different in $YMn_4Al_8$.

The $^{27}$Al spectrum at the elevated temperature in Fig. 8 clearly shows the resolved peaks from two different sites with five peaks. Similar to the magnetic field in the perpendicular direction, this again confirms the existence of two sites for $^{27}$Al in $YMn_4Al_8$. In this figure, the linewidth of the Al-$A$ peak is much narrower than that of the Al-$B$ peak. It should be noted that the $^{27}$Al NMR linewidths for the Al-$B$ peak are 1.7 and 2.0 times larger for the perpendicular and parallel directions, respectively, than those for the Al-$A$ peak. Furthermore, we observed that the spin-lattice relaxation rate $1/T_1$ is larger for the Al-$B$ peak. Because the different crystallographic environments at the Al($8i$) and Al($8j$) sites create different linewidths and relaxation rates for each Al site, we conclude that the Al-$B$ peak is associated with the Al site located closer to a Mn site and strongly influenced by the Mn $3d$ local moments. Therefore, the larger linewidth and $1/T_1$ of the Al-$B$ peak confirms that the Al-$B$ peak originates

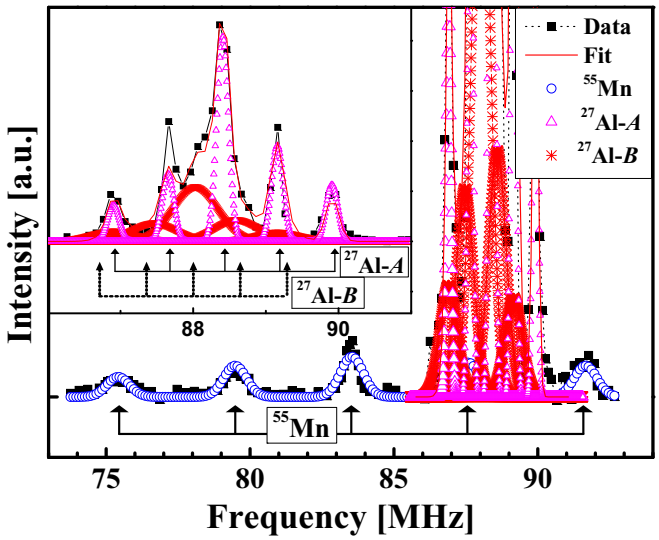


FIG. 8. $^{55}$Mn and $^{27}$Al NMR spectra of $YMn_4Al_8$ at 290 K with a magnetic field of 8.0 T parallel to the $c$ axis. The fit line is a simulated spectrum for the first-order quadrupolar splitting of two $I = 5/2$ nuclei. Three sets of five peaks are shown as guides.

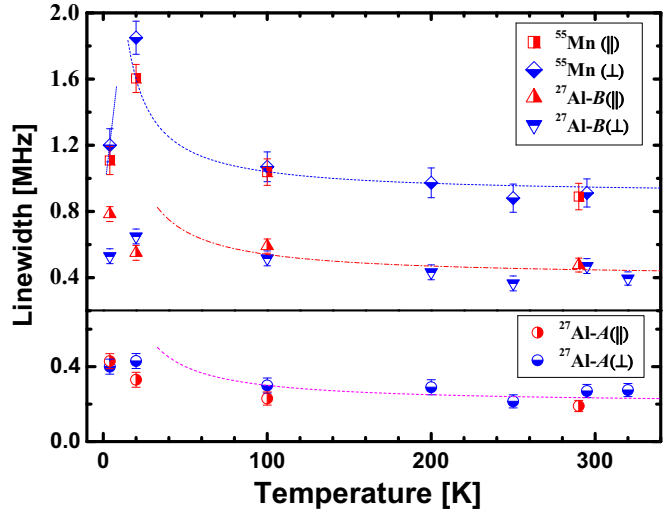


FIG. 9. Temperature dependencies of the $^{55}$Mn and $^{27}$Al linewidths for magnetic fields parallel and perpendicular to the $c$ axis. The lines are drawn as guides for the Curie increases of the Mn, Al-$B$, and Al-$A$ peaks and for the decrease below 20 K.

from the Al($8j$) sites. The inhomogeneous broadening and relaxation rate at the Al sites for both Al-$A$ and Al-$B$ peaks are dominated by the Mn $3d$ local moment.

All $^{55}$Mn and $^{27}$Al NMR spectra were measured at 4–320 K with a magnetic field of 8 T perpendicular and parallel to the $c$ axis. Each spectrum was analyzed to obtain NMR data such as the Knight shift [17], linewidth, and $\nu_Q$ at the $^{55}$Mn and $^{27}$Al nuclear sites. For both directions, as the temperature decreases, the linewidth rapidly increases because the paramagnetic susceptibility increases at low temperatures. Additionally, the respective central peak positions of the $^{55}$Mn and $^{27}$Al NMRs move toward the high-frequency side, indicating the increase in the Knight shift for both nuclei. The $^{55}$Mn NMR intensity decreases dramatically at elevated temperatures because of the faster decay of nuclear spin relaxation.

Figure 9 shows the $^{55}$Mn and $^{27}$Al linewidths versus the temperature. The increasing linewidths for both $^{55}$Mn and $^{27}$Al NMR in the low-temperature range down to 20 K originate from the inhomogeneous broadening owing to paramagnetic impurities, as in the case of the Curie upturn of the susceptibility. However, below 20 K, the linewidth of $^{55}$Mn substantially *decreases*. This anomalous decrease clearly indicates a reduction in the local field inhomogeneity, which may arise from a different configuration of local moments or magnetic ordering. In this regard, it may be noted that $\rho_{\parallel}(T)$ has a local minimum at $T = 15$ K after which it increases, showing semiconducting behavior [3] below 15 K.

The temperature dependence of the frequency separation, $\Delta\nu$, between the central and adjacent satellite peaks is shown in Fig. 10. A comparison of Figs. 4 –6 with Figs. 7 and 8 indicates that $\Delta\nu$ becomes twice as large for the parallel direction, namely, $\Delta\nu(H_0 \parallel c) \approx 2\Delta\nu(H_0 \perp c)$ for $^{55}$Mn NMR. This strongly supports that the principal axis of the EFG tensor at the $^{55}$Mn site is the $c$ axis with an asymmetry factor $\eta \approx 0$, which can be visualized in Fig. 2(a). Therefore, the quadrupole resonance frequency is determined to be $\nu_Q \approx \Delta\nu(H_0 \parallel c) \approx 2\Delta\nu(H_0 \perp c) \sim 3.8$ MHz. However, the same comparison for $^{27}$Al NMR does not show such a relation. Rather, $\Delta\nu$ for the two directions appears to be unrelated; that is, as the $c$ axis is rotated with respect to the external magnetic field $H_0$, the principal axis of the EFG tensor at the $^{27}$Al site seems to show no angular dependence on the direction of the external field. This fact strongly supports that the principal axis of the EFG tensor at the $^{27}$Al nucleus is *not* the $c$ axis, as illustrated in Figs. 2(b) and 2(c). Another possibility is that the asymmetry factor of the EFG tensor for $^{27}$Al is $\eta \neq 0$ and/or $\eta \approx 1$, where the satellite position [15,16] depends on both the polar angle $\theta$ and azimuthal angle $\phi$, generating a complex equation for $\nu_m(\theta, \phi)$.

To understand the angular variation of $^{55}$Mn and $^{27}$Al spectra, we calculated the principal axis of the EFG tensor at the $^{55}$Mn, $^{27}$Al-$A$, and $^{27}$Al-$B$ sites, using VASP. We found

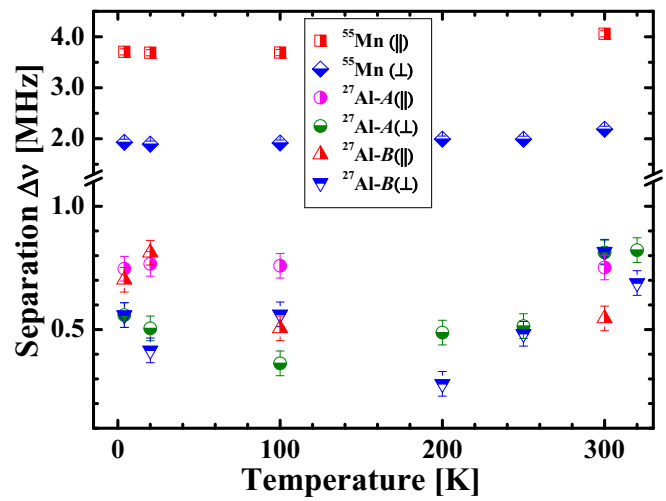


FIG. 10. Temperature dependence of the frequency separation $\Delta\nu$ between resonance peaks for $^{55}$Mn and $^{27}$Al NMR in $YMn_4Al_8$.

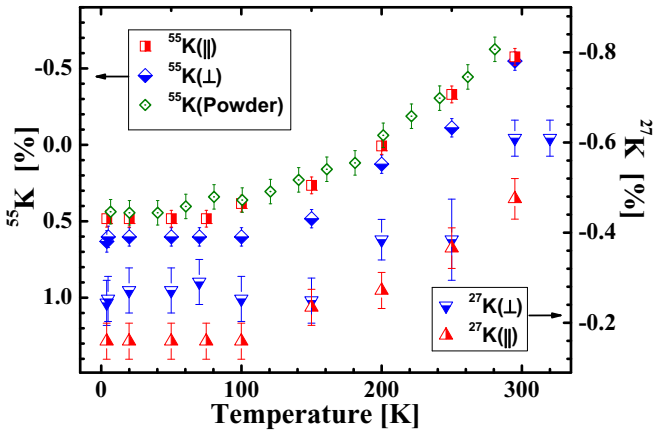


FIG. 11. Temperature dependencies of the Knight shifts for $^{55}$Mn and $^{27}$Al NMR of $YMn_4Al_8$. The powder data are taken from Ref. [1].

that the principal axis of the EFG tensor for $^{55}$Mn is close to the $c$ axis with $\eta \approx 0.13$, whereas those at the Al sites are the $a$ axes with $\eta \approx 0.14$ and 0.81 for $^{27}$Al-$A$ and $^{27}$Al-$B$, respectively. The local symmetry in Fig. 2 also supports this argument [18]. Thus, we understand why the $c$-axis rotation does not lead to a dramatic change; the principal axes of the EFG tensor for both $^{27}$Al sites are not the $c$ axes, and $\Delta\nu$ shows only a different or unrelated variation. Although we cannot determine $\nu_Q$ for $^{27}$Al NMR from Fig. 10, we know that $\nu_Q$ is approximately of the same order as $\Delta\nu(\theta)$; hence, $^{27}\nu_Q \approx 0.4-0.7$ MHz, which is much smaller than $^{55}\nu_Q$. Thus, the large value of $^{55}\nu_Q$ is partially due to the large quadrupole moment [19] $Q$ of the $^{55}$Mn nucleus compared with that of $^{27}$Al; that is, $^{55}Q/^{27}Q = 3.7$. Because $\nu_Q$ is determined by the product of $Q$ and the EFG tensor, the other possibility may be the large EFG at the $^{55}$Mn site.

### B. NMR Knight shifts and hyperfine coupling constants

In Figs. 4 –8, the central peak position $\nu_n$ defines the Knight shift [17], $K \equiv (\nu_n - \nu_0)/\nu_0$, relative to the unshifted position of $\nu_0 = \gamma_n H_0$, where $\nu_n$ is the frequency of the central peak at an applied magnetic field $H_0$ and $\gamma_n$ is the gyromagnetic ratio of the resonant nucleus, e.g., $^{55}\gamma$ for $^{55}$Mn. The electron spin polarization often generates an additional field, the so-called averaged hyperfine field $\langle H_{\rm hf}\rangle_{\rm av}$, at the nucleus; the center frequency of the NMR peak thus appears shifted in frequency at $\nu_n = \gamma_n\{H_0 + \langle H_{\rm hf}\rangle_{\rm av}\}$. Thus, the Knight shift measures the hyperfine field generated by the spin polarization of conduction electrons by an external field, namely, $K = \langle H_{\rm hf}\rangle_{\rm av}/H_0$, which is proportional to the DOS at the Fermi energy $E_F$. The typical Knight shift of a metallic sample is a small percentage value, for example, $K = +0.237\%$ for the $^{63}$Cu NMR spectrum of metallic Cu [19].

Figure 11 shows the temperature dependencies of the Knight shifts for the $^{55}$Mn and $^{27}$Al NMR of $YMn_4Al_8$. As an example for the perpendicular direction of the magnetic field, the $^{55}$Mn NMR Knight shift $^{55}K = +0.61\%$ at 4 K represents a significant change from $-0.55\%$ at 295 K; similarly, the $^{27}$Al NMR Knight shift $^{27}K = -0.26\%$ at 4 K also represents a noticeable change from $-0.61\%$ at 295 K. From the figure, it is obvious that both the $^{55}$Mn and $^{27}$Al NMR Knight shifts show the same behavior as that of the magnetic susceptibility in Fig. 3, namely, a decrease of $-K$ at a low temperature. Because the reduction in the susceptibility supports the decrease in the DOS and confirms the opening of the pseudogap, the $^{55}$Mn and $^{27}$Al NMR Knight shift data also strongly indicate spin pseudogap formation. However, the pseudogap formation is incomplete, and a residual and finite DOS remains below ~100 K.

In Fig. 11, we compare our $^{55}K$ data with the previous powder data [1]. Although the powder average of our anisotropic $^{55}K_{||}$ and $^{55}K_{\perp}$ data is slightly different from the powder data, it is noted that the trends of the temperature dependence are consistent. The small difference seems to originate from the different choice of the NMR reference $\nu_0$. At this point, we note that because the original susceptibility data often show a Curie increase at a low temperature due to the presence of paramagnetic impurities a reduction in the susceptibility is observed only after the Curie upturn is subtracted. In addition, it was reported that the *extrinsic* Curie upturn [12,20] is amplified for disordered and/or non-stoichiometric specimens, whereas the Curie term is *small* for stoichiometric and high-quality polycrystalline $YMn_4Al_8$. Indeed, for the single-crystal sample used in this paper, the Curie upturn in the susceptibility is found to be *small*; in addition, a Curie term (increase) was *never* observed in the $^{55}$Mn and $^{27}$Al NMR Knight shifts. Because NMR is sensitive to the local electronic structures at a nucleus and the intrinsic magnetic moments can generate both Knight shifts, no changes in $^{55}K$ and $^{27}K$ strongly suggest that the Curie upturn of the susceptibility must have been caused by magnetic impurities and is extrinsic in origin.

In general, the measured Knight shifts in metallic samples mainly consist of the spin and orbital parts, i.e., $K(T) = K_{\rm spin}(T) + K_{\rm orb}$. Because only $K_{\rm spin}(T)$ is related to the spin excitations and pseudogap formation, we need to extract $K_{\rm orb}$ by decomposing the measured Knight shift. Considering that both parts have different signs and temperature dependence, we are able to separate each part; these procedures are described in the Appendix. As a result, we find that $^{55}K_{\rm orb}(\perp) \approx +1.53\%$ and $^{55}K_{\rm orb}(||) \approx +1.40\%$, whereas $^{27}K_{\rm orb}(\perp) \approx 0\%$ and $^{27}K_{\rm orb}(||) \approx +0.12\%$. Both orbital shifts for Mn are reasonable compared to the orbital shift of approximately $+1.0\%$ for metallic Mn [19]. The same is also true for Al.

Next, we discuss the anisotropy and error bars of the $K(T)$ data in Fig. 11. $^{55}K$ shows some anisotropy, i.e., $^{55}K_{\perp} > {}^{55}K_{\parallel}$. However, Fig. 11 shows that $^{27}K_{\perp} < {}^{27}K_{\parallel}$. This difference originates from the respective anisotropies in the orbital shift, $^{55}K_{\rm orb}$ and $^{27}K_{\rm orb}$. We note that the $^{27}K$ data have a larger error. This error originates from the overlap between the $^{27}$Al NMR spectra of the Al-$A$ and Al-$B$ peaks, as shown in Figs. 4 –8.

Because the Knight shift is a direct measure of the electron spin polarization at the probed nuclear site, $K$ is proportional to the local DOS at $E_F$ and often follows a linear relation with the spin susceptibility, i.e., $K = A\chi$, where $A$ is the hyperfine coupling constant. As $K$ and $\chi$ have various contributions, $A$ also consists of several parts; for example, $A$ from the

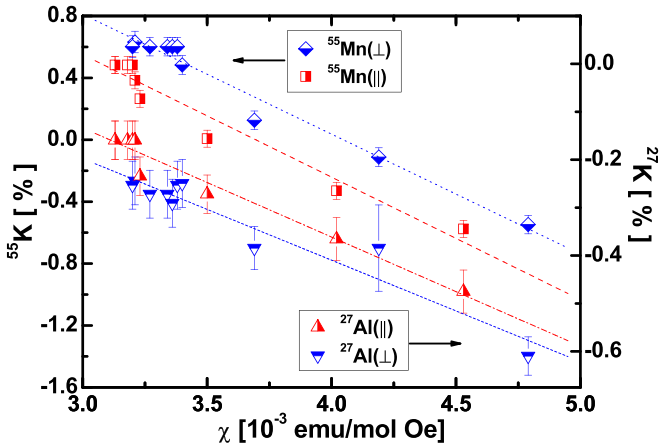


FIG. 12. Plots of $^{55}$Mn and $^{27}$Al NMR Knight shifts vs the susceptibility of $YMn_4Al_8$ for magnetic fields parallel and perpendicular to the $c$ axis. The lines are linear fits to obtain the respective hyperfine coupling constants.

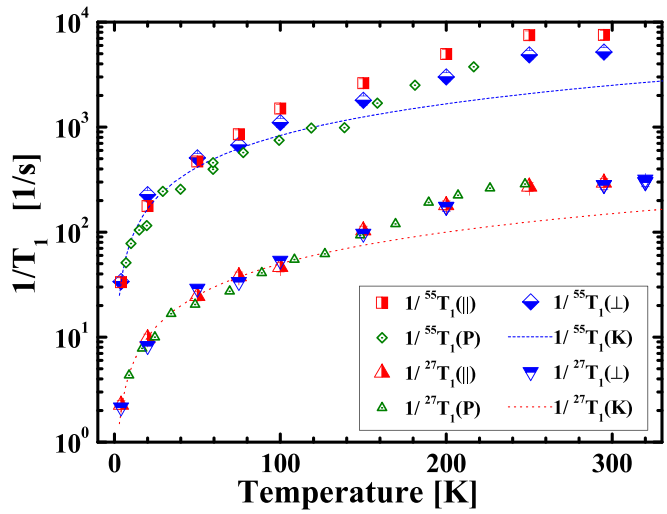


FIG. 13. Temperature dependence of $1/T_1$ for $YMn_4Al_8$. The letter P represents the powder data taken from Ref. [1]. The lines are drawn as guides for the Korringa behavior, $\sim T$. The error bars are equal to the size of the symbols.

spin part due to the core polarization [21] and transferred hyperfine field [19], $A_{\rm spin}$, is often negative for the spin part of susceptibility, $\chi(T)$. Indeed, by plotting $-K(T)$ versus $\chi(T)$ with temperature as an implicit parameter, we obtain linear behaviors for both the $^{55}$Mn and $^{27}$Al NMR Knight shifts, as shown in Fig. 12. From the figure, the hyperfine coupling constants are determined to be $^{55}A_\perp \approx -173 \pm 16\,\text{kOe}/\mu_B$ and $^{55}A_{||} \approx -177 \pm 22\,\text{kOe}/\mu_B$ for $^{55}$Mn NMR, whereas $^{27}A_\perp \approx {}^{27}A_{||} \approx -51 \pm 8\,\text{kOe}/\mu_B$ for $^{27}$Al NMR. We note that both $^{55}A$ and $^{27}A$ are nearly isotropic because of the nature of the $s$ electron at the origin. These values agree with the typical values of the on-site and the transferred hyperfine fields by the core polarization [21] and the Ruderman-Kittel-Kasuya-Yosida (RKKY) interaction [19], respectively. The hyperfine fields at the Mn and Al nuclear spins arise mainly from the 3$d$ orbitals of the Mn atom.

The total hyperfine field at the $^{55}$Mn site, $^{55}A$, has two contributions, intra-atomic and interatomic, with their respective hyperfine coupling constants, namely, the on-site component $^{55}A_{\rm on}$ of the Mn 3$d$ spins and the transferred part $^{55}B_{\rm tr}$ from the *two* neighboring Mn 3$d$ moments *antiferromagnetically coupled* along the 1D dimeric chain, as shown in Fig. 2(a). On the other hand, the total hyperfine field at the $^{27}$Al site, $^{27}A$, has only a transferred contribution $^{27}B_{\rm tr}$ from the *four* neighboring Mn 3$d$ orbitals, as shown in Figs. 2(b) and 2(c). Thus the relative strength of the total hyperfine field at the $^{55}$Mn and $^{27}$Al sites is $^{55}A/{}^{27}A = (^{55}A_{\rm on} + {}^{55}B_{\rm tr})/{}^{27}B_{\rm tr} \approx 3.4$. This is expected because Mn is magnetic but Al is nonmagnetic.

### C. NMR relaxation rates and Korringa ratios

Figure 13 plots the relaxation rates of $^{55}$Mn and $^{27}$Al NMR as a function of the temperature. The spin-lattice relaxation rates, $1/T_1$, for both NMRs were obtained from Eq. (1) $1 - M(t)/M(\infty) = [\alpha\ \exp(-15t/T_1) + \beta\ \exp(-6t/T_1) + \{1 - \alpha - \beta\}\exp(-t/T_1)]$ for the magnetic relaxation [22] of the nuclear spin $I = 5/2$, where $M(t)$ is the magnitude of the NMR signal at time $t$ after the comb pulse. The comb pulse was carefully adjusted to saturate the central transition only. With special consideration for the comb pulse, the fitting coefficients are found to be generally consistent [22] for both $^{55}$Mn and $^{27}$Al nuclei.

For both NMRs, the fast relaxation rates (short decay times) at room temperature exhibit a dramatic (considering the logarithmic scale) decrease down to ~100 K, where they begin to follow the Korringa behavior [15,16], $1/T_1 \propto T$. The Korringa behavior originates from the flip-flop scattering mechanism [19] of nuclear spins by itinerant electrons and it is commonly observed in metallic compounds without paramagnetic moments. Because the spin-lattice relaxation rate $1/T_1$ is a measure of the fluctuating component of the hyperfine field and proportional to the local dynamic susceptibility at the probing nuclear site, $1/(T_1T)$ also scales with the DOS. Thus, the *significant* reduction in $1/T_1$ from room temperature down to ~100 K toward the linear temperature dependence $\sim T$, as shown in Fig. 13, is highly indicative of a gap opening. The reduction in the temperature dependencies of both $^{55}1/T_1$ and $^{27}1/T_1$ and the decrease in $K$ down to ~100 K have the same origin in that the Mn 3$d$ spin dynamics dominate the *fluctuating* part (relaxation rates) as well as the *static* part (hyperfine fields) at both Mn and Al sites.

The high relaxation rate $^{55}1/T_1$ with anisotropy in Fig. 13 supports the fact that the spin-lattice relaxation of the nuclear spin magnetization is mainly dominated by the on-site magnetic excitations $^{55}A_{\rm on}$. In addition, the fluctuation component of the hyperfine field transferred from the two neighboring Mn 3$d$ spins along the 1D chain, $^{55}B_{\rm tr}$, also contributes to the relaxation. However, the values of $^{27}1/T_1$ for both directions are *suppressed* by approximately 20 times compared with the $^{55}$Mn NMR. This significant reduction in the $^{27}1/T_1$ rate suggests the substantial decrease in $H_{\rm hf}$ ($\nu_n$) at the Al sites, which is given by the hyperfine field transferred from Mn 3$d$ spins, $^{27}B_{\rm tr}$. We note that this is a very large suppression in the $^{27}1/T_1$ rate, even under the huge influence of the Mn 3$d$ moment SFs as the nearest neighbor of the Al site. Such a reduction in $1/T_1$ is often significantly manifested

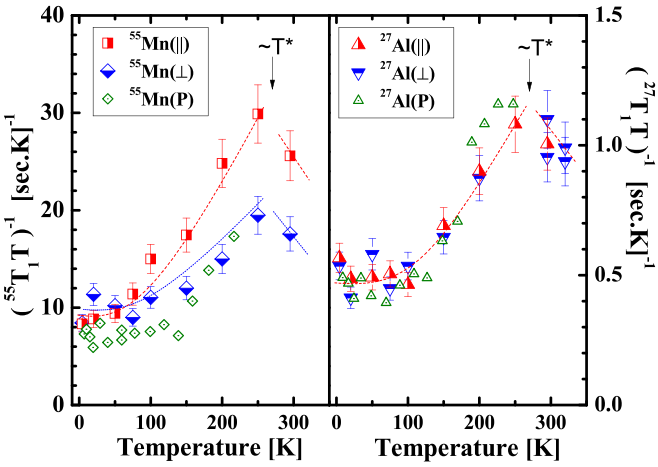


FIG. 14. Temperature dependencies of $1/(^{55}T_1T)$ and $1/(^{27}T_1T)$ for $YMn_4Al_8$. The letter P in the legends represents the powder data taken from Ref. [1]. The lines are drawn as guides to emphasize the reduction in the density of states at the Fermi energy. Below ~100 K, the data are independent of the temperature, showing Korringa behavior as for a finite density of states.

by the geometric cancelation of the antiferromagnetic (AF) SF of Mn 3*d* moments. For example, if the Mn 3*d* SF is correlated antiferromagnetically and the Al atoms are located at the centers of the squares consisting of four Mn atoms, the geometric form factor partially cancels the fluctuating hyperfine fields from the other Mn 3*d* moment on the opposite side. Similar cases are also observed for $^{17}1/T_1$ of $^{17}$O NMR with the cancelation of the AF Cu 3*d* SF in high-$T_c$ cuprates [23,24].

Because $1/T_1$ is proportional to $\{\gamma_n H_{hf}(\nu_n)\}^2 \propto \{\gamma_n A_{spin}\}^2$, where $H_{hf}(\nu_n)$ is the fluctuating hyperfine field at the NMR frequency $\nu_n$ and $A_{spin}$ is the spin part of the hyperfine coupling constant, by using $^{55}\gamma/^{27}\gamma = 0.9465$ and $^{55}A_{spin}/^{27}A_{spin} = (^{55}A_{on} + {}^{55}B_{tr})/^{27}B_{tr} \approx 3.4$ due to the hyperfine field difference at the Mn (*on-site* and *transferred*) and Al (*transferred only*) sites, we find that suppression is expected by a factor of $20/(0.9465 \times 3.4)^2 = 1.93 \approx 2$. Thus, the weaker hyperfine field at the Al sites explains most of the reduction in $^{27}1/T_1$ except for the factor of ~2. This remaining factor seems to originate from the geometric cancelation of the hyperfine field at the Al sites. This factor is also supported by the Korringa ratio difference between the $^{55}$Mn and $^{27}$Al sites, which will be shown later. Therefore, $^{55}1/T_1$ is dominated mostly by the *on-site* Mn 3*d* SF, whereas $^{27}1/T_1$ is suppressed by the *weak transferred* hyperfine field and the *geometric cancelation* of the AF fluctuation of the neighboring Mn 3*d* moments.

Figure 14 shows the temperature dependence of $1/(T_1T)$ for $^{55}$Mn and $^{27}$Al NMR. A rapid decrease of $1/(T_1T)$ for both NMRs is observed at low temperatures, which obviously indicates a gap opening because $1/(T_1T)$ is proportional to the DOS at $E_F$. Although typical simple metals generally exhibit temperature-independent Korringa behavior, i.e., $1/(T_1T) \sim$ constant, metallic $YMn_4Al_8$ displays a variation in $1/(T_1T)$. Thus, Fig. 14 confirms that a considerable suppression in the DOS starts to occur below ~270 K and then stops at approximately 100 K, below which the spin pseudogap does not open completely and a finite DOS remains at $E_F$.

In this regard, we note that the spin excitation gap of 27 meV has been observed by inelastic neutron scattering [25] for $YMn_4Al_8$. However, the spin gap in neutron scattering appears *only* in a limited range of wave vectors, $|Q| \geqslant 3\,\text{Å}^{-1}$, which is an important fact for the NMR data. Although neutron scattering also measures the spin excitation and spin arrangements, NMR probes the spin susceptibility at a different time scale, spatial range, and energy. In other words, NMR is a local probe that is very sensitive to the neighborhood of a probing nuclear spin, which means that both the Knight shift and $1/(T_1T)$ are determined by $\chi(q,\omega)$. Therefore, the spin gap in the limited range of wave vectors $q$ in neutron scattering agrees with the *incomplete* gap opening and finite DOS remaining at low temperatures. This observation of the *residual* DOS is consistent with our results as well as previous NMR results [1]. In addition, considering the site-sensitive aspects of NMR measurements and the significant values of both $^{55}K$ and $^{55}1/(T_1T)$ below 100 K for our *single-crystal* sample, we conclude that the *residual* DOS, after the pseudogap opening stops before completion, is *intrinsic* in $YMn_4Al_8$.

Now, we focus on the anisotropy of $1/(T_1T)$ during the pseudogap opening, as shown in Fig. 14. For the $^{55}$Mn NMR, the anisotropy is roughly $^{55}1/(T_1T)_{\parallel}/^{55}1/(T_1T)_{\perp} \approx 1.35$–$1.65$ for $100 < T < 295$ K. Because $^{55}1/(T_1T)_{\parallel}/^{55}1/(T_1T)_{\perp} = 2\,{}^{55}A_{\perp}{}^2\chi''_{\perp}/(^{55}A_{\perp}{}^2\chi''_{\perp} + {}^{55}A_{\parallel}{}^2\chi''_{\parallel})$, using the nearly isotropic $^{55}A$, namely $^{55}A_{\perp} \approx {}^{55}A_{||}$ from the analysis of $^{55}K(T)$ versus $\chi(T)$ in Fig. 12, we find that the anisotropy of $\chi''$, the imaginary part of $\chi(q,\omega)$, increases up to a factor of $\chi''_{\perp}/\chi''_{\parallel} \approx 4.7$ at $T \approx 200$ K during the gap opening in the temperature range of $100 < T < 295$ K. This is a significant anisotropy developed through gap formation. Thus, we conclude that this significant anisotropy of $\chi''$ (strong enhancement of $\chi''_{\perp}$ in-plane SF) originates from the 1D nature of the Mn magnetic interaction along the $c$ axis. As the temperature decreases further below 100 K, the gap formation stops before completion and a finite DOS remains; consequently, $^{55}1/(T_1T)$ becomes constant around the lowest temperature, suggesting that the AF SF is suppressed in $YMn_4Al_8$, and then becomes an itinerant electron metal in the ground state. Unlike $^{55}$Mn NMR, the $^{27}1/(T_1T)$ rate is isotropic, which is consistent with the Korringa ratios of the Al sites shown later. The reason for this seems to be the transferring mechanism of the Mn 3*d* hyperfine field toward the Al-*A* and Al-*B* sites.

We now address the pseudogap temperature $T^*$ at which the pseudogap begins to open. According to the large amount of NMR data showing pseudogap opening, $T^*$ is often reported as the peak temperature of $1/(T_1T)$ for the NMR measurements [26]. Based on the peak temperatures of $^{55}1/(T_1T)$ and $^{27}1/(T_1T)$ in Fig. 14, $T^*$ is found to be approximately 270 K. This value of $T^*$ is supported by the electric resistivity [3] $\rho(T)$ of $YMn_4Al_8$, which deviates from the linear behavior, $\sim T$, and shows a faster decrease below ~270 K. This coincidence is also observed in high-$T_c$ cuprates [26]. We note that the pseudogap temperature $T^*$ appears differently in $K(T)$ and $1/(T_1T)$ because $K$ and $1/(T_1T)$ are determined by a different part of spin susceptibility, as explained below.

Although the observation of the pseudogap and the identification of $T^*$ are known to be dependent on the experimental techniques used, this agrees with the typical values [26] of $T^*$ in high-$T_c$ cuprates, where the origin of pseudogap is under debate.

Because $1/T_1$ is the energy transfer rate from nuclear to electron spins and sensitively probes the local magnetic field fluctuation component at the NMR angular frequency of $\omega_n$, it is related to the imaginary part of the dynamic spin susceptibility as follows: $1/T_1 = (\gamma_n^2 k_B T/2\mu_B{}^2)\sum_q |A_{\rm spin}(q)|^2 \chi''(q,\omega_n)/\omega_n$, where the summation is conducted over the Fermi surface [15,19]. Because $\omega_n$ is very small compared to the characteristic scale of the electron energy levels, it is approximated as $\omega_n \sim 0$. On the other hand, the value of $K_{\rm spin}$ depends on the real part of the static spin susceptibility with $K_{\rm spin} = A_{\rm spin}(0)/\mu_B \chi'(0,\ 0)$.

For a simple metallic band where the contact term is a dominant source of the Knight shift and spin-lattice relaxation rate $1/T_1$, the so-called Korringa product [19], $T_1 T K_{\rm spin}(T)^2$, is often constant and equal to $S \equiv \hbar(\gamma_e/\gamma_n)^2/(4\pi k_B)$. Therefore, the Korringa ratio, defined as $\xi(T) \equiv T_1 T K_{\rm spin}(T)^2/S$, is often equal or close to unity for simple metals such as alkali metals [19]. However, even for simple metals, a deviation from unity arises from various sources. Electron correlations are a common reason for the deviation because they influence $K$ and $T_1T$ differently. In some transition metals, the exchange enhancement is sufficiently strong to produce a negative $K$ and the $s$-$d$ core polarization becomes a dominant mechanism for the electron-nuclear interaction. As a result, $\xi$ becomes larger owing to the orbital degeneracy at the Fermi energy [19]. In addition, the Korringa ratio often shows different behavior depending on the type of magnetic interaction in correlated electron systems. For magnetically correlated systems, the dynamic spin susceptibility $\chi(q,\omega)$ has a $q$ dependence with an enhancement at $q = 0$ for ferromagnetic (FM) metals and $q = Q_{\rm AF}$ for AF conductors. For the FM case, $K$ is enhanced, but $1/T_1T$ becomes smaller because $\chi(q,\omega)$ is reduced at $q \neq 0$. Thus, the Korringa ratio $\xi$ becomes larger than unity. On the other hand, $\chi(q,\omega)$ for AF metals has a peak at $q = Q_{\rm AF}$ so that the static susceptibility and $K$ are reduced, whereas $1/T_1T$ is enhanced so that $\xi$ becomes smaller than unity.

$K$ reflects the static hyperfine field along the external magnetic field, whereas $1/T_1$ probes the fluctuating hyperfine field perpendicular to the direction of the magnetic field. Thus, the appropriate Korringa ratio is modified for systems with an anisotropic magnetic interaction; because $1/(T_1T)_\parallel \propto 2A_\perp^2 \chi''_\perp \propto 2K_\perp^2$ and $1/(T_1T)_\perp \propto A_\perp^2 \chi''_\perp + A_\parallel^2 \chi''_\parallel \propto K_\perp^2 + K_\parallel^2$, $\xi(\perp) \equiv 2(T_1T)_\parallel K_\perp^2/S$ and $\xi(||) \equiv K_\parallel^2/[\{1/(T_1T)_\perp - 1/(2T_1T)_\parallel\}S]$.

Figure 15 shows the temperature dependence of the Korringa ratio $\xi(||)$ and $\xi(\perp)$ for both $^{55}$Mn and $^{27}$Al NMR. If $K$ and $1/(T_1T)$ are dominated by the contact interaction and a correlation is absent, as seen in simple metals, the Korringa ratio $\xi$ is temperature independent and close to unity. However, when a noncontact contribution such as the $s$-$d$ core polarization dominates, the Korringa ratio deviates from unity. Above 100 K, $^{55}\xi$ is temperature dependent, much larger than

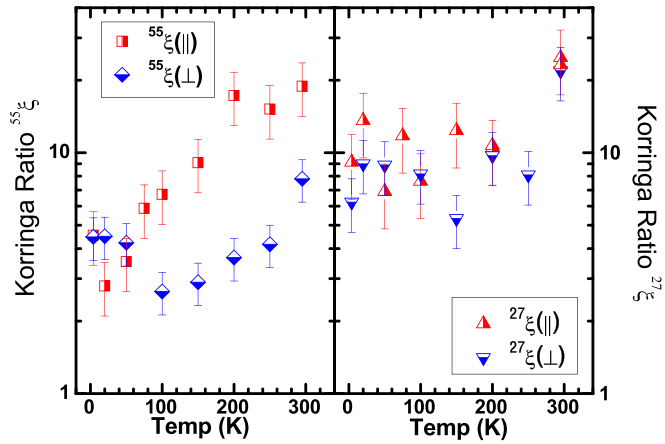


FIG. 15. Temperature dependence of the Korringa ratio $\xi$ for $^{55}$Mn and $^{27}$Al NMR of $YMn_4Al_8$.

unity, and highly *anisotropic*, and $^{55}\xi(||) > {}^{55}\xi(\perp)$ by a factor of 2.5–4.7. However, at lower temperatures $^{55}\xi$ decreases toward unity, and becomes *isotropic* and constant below 100 K, whereupon the pseudogap opening stops before it is completed and the residual DOS remains. On the other hand, $^{27}\xi$ is also much larger than unity but weakly temperature dependent and almost isotropic within the experimental error throughout all experimental temperatures. Below 100 K, $^{27}\xi$ is larger than $^{55}\xi$ by a factor of ~2 for both directions. This factor originates from the geometrical cancelation of the AF SF of Mn 3$d$ moments at the Al sites, as discussed previously for $1/(T_1T)$ in Fig. 13. Both Korringa ratios do not show a reduction by the AF correlation, which presumably results from the AF spin-gap opening [25].

## IV. CONCLUSION

To study the local electronic structures at the Mn and Al sites associated with the pseudogap opening in $YMn_4Al_8$, we performed magnetic susceptibility and $^{55}$Mn and $^{27}$Al NMR measurements on a single-crystal sample over a temperature range of 4–320 K. The NMR spectrum, Knight shift, linewidth, and spin-lattice relaxation rate $1/T_1$ were measured as functions of the temperature for the $c$ axis, which is parallel and perpendicular to the field of 8 T. The $^{55}$Mn and $^{27}$Al NMR spectra display the three sets of five peaks by nuclear quadrupole perturbation of the nuclear Zeeman splitting of $I = 5/2$. The $^{27}$Al NMR spectrum exhibits two different peaks, Al-$A$ and Al-$B$. On the basis of the much broader linewidths and larger $1/T_1$ of the Al-$B$ peak, the Al-$B$ peak is identified as originating from the Al(8$j$) site, closer to the Mn 3$d$ moments, and the Al-$A$ peak is assigned to the Al(8$i$) site.

The temperature dependencies of $K$ and $1/(T_1T)$ for both NMRs show a large decrease with decreasing temperature, similar to the susceptibility, indicating the opening of a pseudogap down to 100 K, where spin pseudogap formation stops before it is completed and a finite DOS remains below. A plot of $-K(T)$ versus $\chi(T)$ clearly confirms that the Knight shifts scale with the susceptibility. From a linear fit of the plot, the hyperfine coupling constants are extracted

as $^{55}A_{\perp} = -173 \pm 16\,\mathrm{kOe}/\mu_B$, $^{55}A_{||} = -177 \pm 22\,\mathrm{kOe}/\mu_B$, and $^{27}A_{\perp} \approx {}^{27}A_{||} \approx -51 \pm 8\,\mathrm{kOe}/\mu_B$.

From the decomposition analysis of Knight shifts in the Appendix, we find that $^{55}K(T)$ and $^{27}K(T)$ are governed respectively by the core polarization and the transferred hyperfine field from the Mn $3d$ spins. In addition, we find that $^{55}K(T)$ is dominated by the *on-site* hyperfine field at the Mn site, whereas $^{27}K(T)$ is affected mostly by the *transferred* hyperfine field of the four neighboring Mn $3d$ spins at the Al sites. The transferred hyperfine fields at $^{27}$Al sites are found to be weaker by a factor of $\sim$3.4 than the hyperfine fields at the Mn sites. By this way, we estimate both orbital shifts, $^{55}K_{\mathrm{orb}}$ and $^{27}K_{\mathrm{orb}}$, for both directions, as shown in the Appendix, and we can extract the spin part of the Knight shift from $^{55}K(T)$ and $^{27}K(T)$ for the calculation of the Korringa ratio.

From the temperature dependencies of $1/(T_1T)$ for both NMRs, the pseudogap temperature $T^*$ is found to be approximately 270 K. Comparing the large value of $^{55}1/(T_1T)$ with the substantial (approximately 20 times) reduction in $^{27}1/(T_1T)$, we conclude that the *on-site* hyperfine field dominates $^{55}1/T_1$, whereas the *weak transferred* hyperfine field determines $^{27}1/T_1$. Moreover, we find that the Mn magnetic interaction is AF and the SF of the Mn $3d$ moments is geometrically canceled by a factor of $\sim$2 at the Al sites.

From the anisotropy of $^{55}1/(T_1T)$ during the pseudogap opening down to $\sim$100 K, we find that the AF SF is anisotropically stronger by up to 4.2 times at $T \approx 200$ K in the basal plane perpendicular to the 1D chain. This is a significant anisotropy developed through gap formation. This substantial anisotropy of $\chi''$ probably originates from the 1D nature of the Mn AF interaction.

Above 100 K, the Korringa ratios at the Mn sites are temperature dependent, much larger than unity, and highly *anisotropic*, and $^{55}\xi(||) > {}^{55}\xi(\perp)$. As temperature decreases, $^{55}\xi$ decreases and approaches unity, becoming *isotropic* and constant below 100 K, whereupon the pseudogap opening stops before it is completed and the residual DOS remains. $^{27}\xi$ is much larger than unity but weakly temperature dependent and almost isotropic within a reasonable experimental error. Below 100 K, $^{27}\xi$ is larger than $^{55}\xi$ by a factor of $\sim$2 for both directions, which seems to result from the geometrical cancelation of the AF SF of the Mn $3d$ moments at the Al sites.

## ACKNOWLEDGMENTS

This work was supported by Konkuk University in 2016. The authors are thankful to Prof. Yunkyu Bang at Asia Pacific Center for Theoretical Physics (APCTP), Republic of Korea, for helpful discussions on the experimental data. We are grateful to Prof. Jaejun Yu and Mr. Seungjin Kang at Seoul National University, Republic of Korea, for the electric-field gradient calculation, and Mr. M. S. Song at Gwangju Institute of Science and Technology, Republic of Korea, for the susceptibility measurements.

## APPENDIX: DECOMPOSITION OF KNIGHT SHIFTS

In general, the NMR frequency shift from a reference position has several sources in metallic compounds; $K(T) = K_{\mathrm{spin}}(T) + K_{\mathrm{nonspin}}$, where $K_{\mathrm{spin}}(T)$ and $K_{\mathrm{nonspin}}$ are the contributions of the spin and nonspin parts of the susceptibility [19], respectively. The respective contribution to the shift is proportional to each part of the susceptibility $\chi$ by the equation $K = A\chi$. To ascertain the local electronic structures and dynamics due to the Mn $3d$ spins, we need to extract the spin contribution $K_{\mathrm{spin}}$ from the measured shift data $K$. $K_{\mathrm{spin}}$ is also important to estimate the so-called Korringa ratio [19]. To separate $K_{\mathrm{spin}}$ from the total shift, we must determine $K_{\mathrm{orb}}$.

$K_{\mathrm{spin}}$ is a direct measure of the spin density at the nucleus; $K \propto |\psi_{\mathrm{F}}(0)|^2$, where $\psi_{\mathrm{F}}(0)$ is the Bloch wave function at the nucleus at the Fermi energy. In short, $K = \mu_B H_{\mathrm{hf}} N(E_{\mathrm{F}})$, where $H_{\mathrm{hf}}$ is the hyperfine field at the nucleus and $N(E_{\mathrm{F}})$ is the DOS at the Fermi energy $E_{\mathrm{F}}$. Because only an $s$-wave electron has a nonzero probability at the origin, the Knight shift primarily depends on the $s$-electron polarization. This intra-atomic polarization process is made possible by the direct polarization of an $s$ electron itself and by an indirect process known as core polarization [21]. The most prominent core-polarization processes occur through $s$-$d$ or $s$-$f$ orbital coupling, which is often observed in transition metals and rare-earth compounds. Other types of $s$-electron polarizations are possible by interatomic processes such as the RKKY and hybridization interactions.

In detail, $K_{\mathrm{spin}}$ consists of several parts—$K_{\mathrm{con}}$, $K_{\mathrm{cp}}$, and $K_{\mathrm{tr}}$. $K_{\mathrm{con}}$ originates from the contact hyperfine field from a nonzero spin density (unfilled $s$-orbital electrons) at the nuclear position and $K_{\mathrm{cp}}$ is the hyperfine field generated by the core-polarization process. $K_{\mathrm{con}}$ is positive and usually temperature independent. $K_{\mathrm{cp}}$ is usually negative and often strongly temperature dependent because $\chi_d$ and $\chi_f$ depend sensitively on the temperature. If $\chi_s$ is small but either $\chi_d$ or $\chi_f$ dominates a magnetic susceptibility, then $K_{\mathrm{con}}$ is small, but $K_{\mathrm{cp}}$ dominates the total Knight shift, leading to a very large and negative $K(T)$ with strong temperature dependence. This behavior is indeed observed for $YMn_4Al_8$ in Fig. 11; that is, $^{55}K(T)$ is very large, negative, and strongly temperature dependent, which reflects that $^{55}K$ is dominated by the $s$-$d$ core-polarization process of the Mn $3d$ moments. On the other hand, the core polarization is small for $^{27}$Al because the $p$ orbital of aluminum is positioned far below the Fermi level. Therefore, the same behavior of $^{27}K(T)$, namely, the large and negative shift with a strong temperature dependence, suggests that $^{27}K$ is mainly influenced by the transferred hyperfine field ($^{27}B_{\mathrm{tr}}$) from the Mn $3d$ spins via RKKY indirect interaction mediated by itinerant electrons.

The nonspin part of the Knight shift consists of two sources, i.e., $K_{\mathrm{nonspin}} = K_{\mathrm{dia}} + K_{\mathrm{orb}}$, where $K_{\mathrm{dia}}$ originates from the diamagnetic field generated by the inner (filled) core orbitals and $K_{\mathrm{orb}}$ arises from the orbital hyperfine field and is proportional to the Van Vleck orbital susceptibility $\chi_{\mathrm{orb}}$ [27]. $K_{\mathrm{dia}}$ is negative and usually much smaller than the other contributions. $K_{\mathrm{orb}}$ is positive and usually small. However, $K_{\mathrm{orb}}$ often becomes very large for transition metals and rare-earth compounds [19], where the $d$ and $f$ orbitals are closely spaced near $E_{\mathrm{F}}$. $K_{\mathrm{dia}}$ remains constant with temperature, and $K_{\mathrm{orb}}$ is temperature independent in most cases [19]. Because $K_{\mathrm{dia}}$ is typically much smaller [19] than the measured $K$ data in Fig. 11, we know that $K_{\mathrm{nonspin}} = K_{\mathrm{dia}} + K_{\mathrm{orb}} \approx K_{\mathrm{orb}}$ for both $^{55}$Mn and $^{27}$Al NMR.

Therefore, the measured Knight shift is composed of the temperature-independent orbital part and the temperature-dependent spin part, i.e., $K(T) = K_{\rm orb} + K_{\rm spin}(T)$. In order to estimate $K_{\rm orb}$, we now focus on the temperature dependence of $K(T)$, i.e., both $K(4\,{\rm K})$ and $\Delta K \equiv K(295\,{\rm K}) - K(4\,{\rm K})$ for the $^{55}$Mn and $^{27}$Al sites. We find that, at $T = 4\,{\rm K}$, $^{55}K(\perp) = +0.608\%$ and $^{55}K(\parallel) = +0.483\%$, whereas $^{27}K(\perp) = -0.266\%$ and $^{27}K(\parallel) = -0.155\%$. For a precise assessment of $K(T)$ at 4 K, we take the average values below 70 K because $K(T)$ is almost independent of the temperature within the experimental error. Because $K_{\rm orb}$ is positive and temperature independent, the measured $K$ data at 4 K must include $K_{\rm orb}$.

Although both $^{27}K_{\rm orb}(\perp)$ and $^{27}K_{\rm orb}(\parallel)$ should be positive, we focus on the fact that both $^{27}K(\perp)$ and $^{27}K(\parallel)$ at 4 K are still negative. Taking into account that the orbital shift of Al *without d* orbitals must be *small* from the above formula of $K_{\rm orb}$, we are able to assume that both $^{27}K_{\rm orb}(\perp)$ and $^{27}K_{\rm orb}(\parallel)$ are *small or negligible*. At this point, it should be emphasized that both $^{55}K_{\rm orb}$ and $^{27}K_{\rm orb}$ can be *anisotropic*, whereas both $^{55}K_{\rm cp}$ and $^{27}K_{\rm tr}$ are *isotropic* because of the *s*-orbital nature. Indeed, we note that the values of $^{27}K(T)$ are almost the same except for a slight difference of ∼0.11 and ∼0.13% at 4 and 295 K, respectively, between the parallel and perpendicular directions. After careful analysis to satisfy the *above* requirements for $^{55}K_{\rm cp}$ and $^{27}K_{\rm tr}$ as well as $^{55}K_{\rm orb}$ and $^{27}K_{\rm orb}$ within a reasonable experimental error, we conclude that $^{27}K_{\rm orb}(\perp) \approx 0\%$ and $^{27}K_{\rm orb}(\parallel) \approx +0.12\%$, leading to $^{27}K_{\rm tr}(\perp) = {}^{27}K_{\rm tr}(\parallel) \approx -0.27\%$ at 4 K and $^{27}K_{\rm tr}(\perp) = {}^{27}K_{\rm tr}(\parallel) \approx -0.60\%$ at 295 K.

Next, we concentrate on the temperature variation $K(T)$, namely, $\Delta K \equiv K(4\,{\rm K}) - K(295\,{\rm K}) = \Delta K$. From the measured data, we find that $\Delta^{55}K(\perp) = -1.156\%$ and $\Delta^{55}K(\parallel) = -1.059\%$, whereas $\Delta^{27}K(\perp) = -0.344\%$ and $\Delta^{27}K(\parallel) = -0.316\%$. Therefore, $\Delta^{55}K(\perp)/\Delta^{27}K(\perp) \approx 3.36$, whereas $\Delta^{55}K(\parallel)/\Delta^{27}K(\parallel) \approx 3.35$. It is noted that the two ratios are very close. This ratio is just the relative strength of the total hyperfine field at the $^{55}$Mn and $^{27}$Al sites. After multiplying $^{27}K_{\rm tr}(\perp)$ and $^{27}K_{\rm tr}(\parallel)$ at 4 K by a factor of 3.4, we are able to estimate that $^{55}K_{\rm cp}(\perp) = {}^{55}K_{\rm cp}(\parallel) \approx -0.92\%$ at 4 K, which means that $^{55}K_{\rm orb}(\perp) \approx +1.53\%$ and $^{55}K_{\rm orb}(\parallel) \approx +1.40\%$. Accordingly, $^{55}K_{\rm cp}(\perp) \approx -2.07\%$ and $^{55}K_{\rm cp}(\parallel) \approx -1.98\%$ at 295 K.


[1] H. Nakamura, S. Giri, and T. Kohara, Pseudo-gap in $YMn_4Al_8$, J. Phys. Soc. Japan **73**, 2971 (2004).

[2] I. H. Hagmusa, J. C. P. Klaasse, E. Brück, F. D. de Boer, and K. H. J. Buschow, A specific-heat study of $RMn_4Al_8$ compounds (R = Y, La, Pr, Nd, Dy, Er), J. Alloy. Compd. **297**, 21 (2000).

[3] J. Y. Kim, J. G. Park, B. K. Cho, and Y. Janssen, Magnetic and electronic anisotropy in single crystalline $YMn_4Al_8$, J. Appl. Phys. **99**, 08F506 (2006).

[4] V. Jaccarino, G. K. Wertheim, J. H. Wernick, L. R. Walker, and S. Arajs, Paramagnetic excited state of FeSi, Phys. Rev. **160**, 476 (1976).

[5] B. D. Rainford, C. J. Leavey, A. D. Hillier, and J. R. Stewart, Magnetic ground states of $RMn_4Al_8$, R = La, Pr, Y, Physica B **359**, 929 (2005).

[6] T. Yamasaki, K. Matsui, H. Nakamura, and M. Shiga, Nearly antiferromagnetic metal with linear spin chains: $LaMn_4Al_8$, Solid State Commun. **119**, 415 (2001).

[7] K. H. J. Buschow, J. H. N. v. Vucht, and W. W. w. d. Hoogenhof, Note on the crystal structure of the ternary rare earth-3d transition metal compounds of the type $RT_4Al_8$, J. Less-Common Met. **50**, 145 (1976).

[8] I. Felner and I. Nowik, Magnetism and hyperfine interactions of $^{57}$Fe, $^{151}$Eu, $^{155}$Gd, $^{161}$Dy, $^{166}$Er and $^{170}$Yb in $RM_4Al_8$ compounds (R = rare earth or Y, M = Cr, Mn, Fe, Cu), J. Phys. Chem. Solids **40**, 1035 (1979).

[9] M. Shiga, Magnetism and spin fluctuations of laves phase manganese compounds, Physica B+C **149**, 293 (1988).

[10] K. H. J. Buschow and A. M. van der Kraan, Magnetic ordering in ternary rare earth iron aluminium compounds ($RFe_4Al_8$), J. Phys. F **8**, 921 (1978).

[11] M. Coldea, M. Neumann, St. Lütkehoff, S. Mähl, and R. Coldea, Spin and valence fluctuations in $CeMn_4Al_8$ and $CeMn_6Al_6$, J. Alloys Compd. **278**, 72 (1998).

[12] A. M. Palasyuk, B. Ya. Kotur, E. Bauer, H. Michor, and G. Hilscher. Electrical conductivity of $ThMn_{12}$- and $Th_2Zn_{17}$-type ternary intermetallic compounds in R–T–Al systems (R = Y, La, Ce, Gd, Tb; T = Mn, Fe), J. Alloys Compd. **367**, 205 (2004).

[13] Y. Janssen, M. Angst, K. W. Dennis, R. W. McCallum, and P. C. Canfield, Differential thermal analysis and solution growth of intermetallic compounds, J. Cryst. Growth **285**, 670 (2005).

[14] E. Fukushima and S. B. W. Roeder, *Experimental Pulse NMR* (Addison-Wesley, Reading, MA, 1981), Chap. 3.

[15] C. P. Slichter, *Principles of Magnetic Resonance*, 3rd ed. (Springer-Verlag, Berlin, 1989).

[16] A. Abragam, *The Principles of Nuclear Magnetism* (Oxford University, New York, 1985).

[17] W. D. Knight, A electron paramagnetism and NMR in metals, in *Solid State Physics*, edited by F. Seitz and D. Turnbull (Academic Press Inc., New York, 1956), Vol. 2, pp. 93–136.

[18] K. Kang, Nuclear magnetic resonance investigation of $YMn_4Al_8$ and $LuAl_2$, Ph.D. Thesis, Konkuk University, 2007.

[19] G. C. Carter, L. H. Bennett, and D. J. Kahan, *Metallic Shifts in NMR*, in Progress in Materials Science, edited by B. Chalmers, J. W. Christian, and T. B. Massalski (Pergamon Press, Oxford, 1977), Vol. 20, p. 295.

[20] B. Ya Kotur, A. M. Palasyuk, E. Bauer, H. Michor, and G. Hilscher, Uncommon conductivity of R–Mn–Al (R = Gd, Tb) ternary compounds, J. Phys.: Condens. Matter **13**, 9421 (2001).

[21] R. E. Watson and A. J. Freeman, in *Hyperfine Interactions*, edited by A. J. Freeman and R. B. Frankel (Academic, New York, 1967), p. 53.

[22] A. Narath, Nuclear spin-lattice relaxation in hexagonal transition metals: Titanium, Phys. Rev. **162**, 320 (1967).

[23] A. J. Millis, H. Monien, and D. Pines, Phenomenological model of nuclear relaxation in the normal state of $YBa_2Cu_3O_7$, Phys. Rev. B **42**, 167 (1990).

[24] P. C. Hammel, M. Takigawa, R. H. Heffner, Z. Fisk, and K. C. Ott, Spin Dynamics at Oxygen Sites in $YBa_2Cu_3O_7$, Phys. Rev. Lett. **63**, 1992 (1989).

[25] C. J. Leavey, B. D. Rainford, J. R. Stewart, and D. T. Adroja, Spin gaps in pseudo-one-dimensional $RMn_4Al_8$ compounds (R = Y, Ce and La), J. Magn. and Magn. Mater. **310**, 1041 (2007).

[26] T. Timusk and B. Statt, The pseudo-gap in high-temperature superconductors: An experimental survey, Rep. Prog. Phys. **62**, 61 (1999).

[27] J. H. van Vleck, The dipolar broadening of magnetic resonance lines in crystals, Phys. Rev. **74**, 1168 (1948).